

Adaptive Subband Compression of Streaming Data for Power System Monitoring and Control

Xinyi Wang, Yilu Liu, and Lang Tong

Abstract—A data compression system capable of providing high-fidelity high-resolution streaming of power system real-time measurements is proposed. Referred to as adaptive subband compression, the proposed technique partitions the signal space into subbands and adaptively compresses subband signals based on each subband's active bandwidth. The proposed technique conforms to existing industry standards for phasor measurement units. It applies to the streaming of phasor measurements or high-frequency point on waveform samples of power system signals. Experiments on synthetic and real data show that the prototyped technology reduces the required communication data rate by several orders of magnitude while maintaining the precision required by the industry standards.

Index Terms—Phasor measurement unit (PMU), power system monitoring and control, subband coding, adaptive data compression.

I. INTRODUCTION

The invention of the phasor measurement unit (PMU) technology in the late '80s was considered a major breakthrough in power systems monitoring and control. By communicating synchronized phasor and frequency measurements at the rate of 60 to 120 measurements per second to the control center, the PMU technology has the potential to revolutionize power system operations by providing fast-timescale signal intelligence and enhanced network resilience.

Despite the substantial investments worldwide, the full potential of the PMU technology has yet been realized. A main reason for this underachievement is that the PMU technology needs to be broadly deployed to be effective. Unfortunately, the cumulative installation of PMU remains limited, sufficient for some high voltage networks, but inadequate for large systems. While the cost of broad deployments of PMUs nontrivial, it is the lack of demonstrated “killer applications” that inhibits the necessary investments for large-scale deployments.

With deep penetration of inverter-based resources that exhibits low inertia and fast timescale characteristics, there are cogent needs for an ultra-high-rate grid measurement technology that provides a kilohertz-level high resolution data streaming [1]. Such a technology has the potential to enable real-time transient stability assessment and wide area real-time control.

Xinyi Wang and Lang Tong ({xw555,lt35}@cornell.edu) are with the School of Electrical and Computer Engineering, Cornell University, USA. Yilu Liu (liu@utk.edu) is with the Department of Electrical and Engineering and Computer Science, The University of Tennessee, Knoxville. This work was supported in part by the National Science Foundation under Grants 1932501 and 1816397

A major barrier for streaming of ultra-high-rate measurement, however, is the network bandwidth required. A direct implementation of high resolution data streaming would require up to ten to one hundred-fold increases of network bandwidth. An enabling technology for the broad deployment of high-resolution data streaming is a compression technique that delivers high-fidelity and high-resolution measurements subject to bandwidth constraints of the existing infrastructure.

A back-of-the-envelope calculation gives a rough estimate of the level of compression required to stream high-resolution data under current communication constraints. The current IEEE standards for PMU [2], [3] recommend that PMU measurements include the possibility of harmonics up to the 50th order, which implies that the maximum bandwidth of the original (source) signal is approximately 3 (kHz). By the Nyquist sampling theorem, the signal should be sampled at 6 (kHz) to achieve perfect reconstruction. If the standard PMU reporting frame rate of 60 samples per second is used for streaming PMU data, a 100 to 1 compression ratio would be required. For a fixed communication bandwidth, higher compression ratio is necessary if the analysis of high resolution transient signals is needed. The existing technologies as reported in a survey [4] do not come close to this level of compression.

Having a high degree of compression is only one metric of consideration. Fundamental to compression of streaming data is a tradeoff among three factors: (i) the degree of compression, (ii) the accuracy of the reconstruction of the source using compressed data, and (iii) the delay associated with the compression and decompression processes. The first two were formalized in an information-theoretic setting as the rate-distortion tradeoff by Shannon [5]. The last is particularly relevant to streaming applications in which encoding and decoding delays are significant design constraints.

A. Related Literature

The need for data compression for power system monitoring goes back at least three decades. Mehta and Russell made one of the earliest contributions in [6], where the authors articulated the needs for compression. They recommended to compress data in the frequency domain by the Fast Fourier Transform (FFT) by discarding high-frequency coefficients.

Discarding high-frequency components may lead to significant distortions when the signal has higher-order harmonics.

Nonetheless, a modification of Mehta and Russell's suggestion by a reverse water-filling strategy can achieve the optimal tradeoff between compression ratio and reconstruction error for Gaussian processes [7]. The caveat for the optimality of the FFT-based compression is that the FFT block size must be arbitrarily large, which conflicts with the low latency requirement of data streaming. When the FFT block size is limited to reduce encoding-decoding latency, the FFT-based compression introduces inter-block distortions that result in the loss of signal details and high reconstruction errors.

There is an extensive literature in data compression for power quality data at digital fault recorders (DFR) [8]–[13]. For such applications, the data sampling rate can be as high as 10MHz. Because the recorded data are only uploaded on-demand, often in a post-event analysis, data must be communicated in high accuracy. Thus lossless compression techniques are often preferred. Block processing techniques such as transforms (FFT and discrete-cosine transform (DCT), wavelet-spline) [6], [12], neural network and fuzzy logic [11], [14], [15], and principal component analysis (PCA) [16] have also been developed.

The literature on the compression of streaming data for power system monitoring and control is limited. See a comprehensive survey on compression techniques for smart grid operations [4], where the authors reported the capabilities of various compression techniques with compression ratio up to 5:1 for lossless compressions. Most relevant to our work are the lossy compressions, categorized by wavelet (and waveform packet) transform techniques, mixed transform, and parametric compression techniques. These state-of-the-art offers a 6 to 16:1 compression ratio at the normalized mean squared error (NMSE) of from -20 to -30 dB.

In a broader context, the idea of subband compression considered in this paper has long been successfully applied in multimedia communications. Most of data-streaming techniques (such as the H.264 group) employ some forms of subband compression. The key to subband compression is to exploit subband properties of the signal: compress in frequency bands where the signal requires the least accuracy. In audio and video compression, it is the perceptual properties of the audio and video signals that play a crucial role in achieving a good tradeoff among compression rate, accuracy, and latency. In this paper, we focus on exploiting the harmonic structure of the power signal for compression.

B. Summary of Results and Contributions

We propose a lossy compression technique for the *high-fidelity and high-resolution* data streaming of measurements for a wide area monitoring system. By high-fidelity, we mean that the source's reconstruction has a low mean-squared error within the specification of industry standards. By high-resolution, on the other hand, we mean that the source signal is sampled at a high frequency to include higher-order harmonics, wideband interharmonics, and wideband transient signals. Our goal is to achieve 100:1 to 1000:1 compression

ratio with a reconstruction accuracy satisfying that required by industrial standards [2], [3].

The proposed technique is referred to as *adaptive subband compression (ASBC)* that compress the measurement adaptively based on a subband decomposition of the spectrum of power signals. ASBC can operate in dual modes. One mode is for monitoring and control in which PMU or direct waveform measurements are streamed to the control center with a relatively small delay. The other is for analysis or when the system is in contingency when the control center requires higher-resolution details in specific harmonic and interharmonic subbands.

Fig. 1 illustrates a conceptual realization of the ASBC technology. ASBC consists of an ASBC encoder for each remote sensing device, and an ASBC decoder at the fusion center*. Together, they form the ASBC codec that provides end-to-end data streaming. Implementations of the ASBC codec are explained in Sec. III-IV.

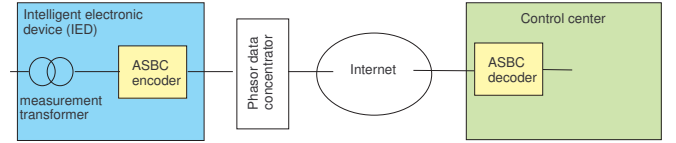


Fig. 1: An application of ASBC technology for high resolution PMU monitoring of power grids.

ASBC partitions the power signal spectrum into harmonic and interharmonic subbands. The harmonic subbands are centered at integral multiples of the system frequency (50 or 60 Hz). Each harmonic subband contains frequency components within the sideband of a specific bandwidth. The interharmonic subband, on the other hand, is a set of frequency bands between harmonic subbands [17].

To achieve a high compression ratio without compromising accuracy, ASBC compresses subband signals adaptively in both time and frequency domains. The encoder monitors the activity levels of subbands and transmits only signals from active subbands. Such an approach is especially useful when some of the subbands are transient in nature. For example, the interharmonic signals are often episodic and have a high bandwidth. The level of interharmonics may be negligible most of the time and becomes strong suddenly when magnified by resonance. Thus an in-situ compression of interharmonics can achieved a high compression ratio without affecting reconstruction accuracy.

II. SIGNAL MODEL AND SUBBAND DECOMPOSITION

We model the continuous-time voltage (or current) signal $x(t)$ as the sum of harmonics $x_k(t)$ and interharmonics $e(t)$:

*A fusion center is the location where data streams from different sensing devices are combined. A fusion center may be located at PMU data concentrators (PDC) or the operator's control center.

$$x(t) = x_0(t) + \sum_{k=1}^K x_k(t) + e(t), \quad (1a)$$

$$x_k(t) = a_k(t) \cos((k+1)\Omega_0 t + \phi_k(t)), \quad (1b)$$

where $x_0(t)$ is the signal component associated with the system frequency F_0 (e.g., 50 or 60 Hz), and $\Omega_0 = 2\pi F_0$. Here we allow $x_0(t)$ and its harmonics $x_k(t)$ to take the general analytical form of (1b). The interharmonic $e(t)$ also models measurement noise outside the harmonic subbands.

Let $X(f)$, $X_k(f)$ and $E(f)$ be the Fourier spectra[†] of $x(t)$, $x_k(t)$, and $e(t)$, respectively, as illustrated in Fig. 2. We assume that the spectrum $X_k(f)$ of the k th harmonic $x_k(t)$ is centered around $(k+1)F_0$ with passband bandwidth[‡] of $W_k < F_0$. The total bandwidth of $x(t)$ is therefore $KF_0 + \frac{W_K}{2} \leq (K + \frac{1}{2})F_0$.

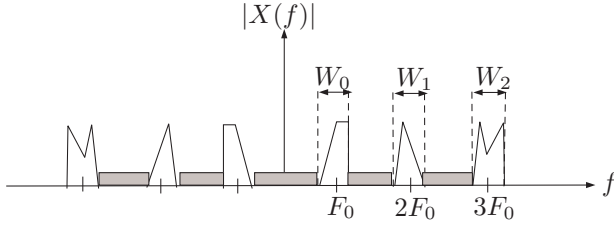


Fig. 2: The spectrum of $x(t)$ and its harmonics. The grey area represents the spectrum of interharmonics.

Sampled at the frequency of $F_s = \frac{1}{T_s} \geq (2K+1)F_0$ (Hz), the discrete-time signal is given by, for $n = 0, \pm 1, \dots$,

$$x[n] := x(nT_s) = x_0[n] + \sum_{k=1}^K x_k[n] + e[k], \quad (2a)$$

$$x_k[n] := a_k[n] \cos\left(\left(k+1\right)\frac{\Omega_0}{F_s}n + \phi_k[n]\right), \quad (2b)$$

where $(a_k[n], \phi_k[n])$ are the sampled amplitude and phase angles and $e[n]$ the interharmonic signal.

III. ADAPTIVE SUBBAND COMPRESSION: ENCODER

As part of the remote terminal unit, the ASBC encoder partitions the signal spectrum into a set of frequency bands. It adaptively masks inactive bands and encodes the unmasked bands in parallel. Fig. 3 illustrates the schematic of the ASBC encoder. The functionalities of individual components are explained below.

[†]Here we assume the existence of Fourier transforms of all signals.

[‡]The *passband bandwidth* is defined by the width of the frequency band containing non zero frequency components.

A. Subband decomposition

From the output of the sensor transformer, the continuous-time measurement signal $x(t)$ is sampled at F_s Hz. The discrete-time signal $x[n]$ is frequency down-shifted and passed through a filterbank $\mathcal{H} = (\mathcal{H}_e, \mathcal{H}_0, \dots, \mathcal{H}_K)$ that extracts the subband signal $x_k[n]$ in its baseband representation $y_k[n]$. Specifically, the output of the k th subband filter is a complex time series

$$y_k[n] = (x[n]e^{-jk\omega_0 n}) \otimes h_k[n], \quad \omega_0 := \frac{2\pi F_0}{F_s},$$

where \otimes is the convolution operator. Ideally, the filter for the k th subband is a low-pass filter with bandwidth $W_k/2$, whose output $y_k[n]$ is the baseband representation of the k th harmonic signal $x_k[n]$, and its continuous-time counter part is $\tilde{x}_k(t) = x_k(t)e^{-jk\Omega_0 t}$.

The interharmonic distortion $y_e[n]$ whose spectrum corresponds to the grey area of power spectrum in Fig. 2 can be extracted by

$$y_e[n] = \sqrt{2}\text{Re}\left(x[n] - \sum_{k=1}^K y_k[n]e^{jk\omega_0 n}\right).$$

In absence of high order and interharmonics, $x(t) = x_0(t)$ in (1), and only $y_0[n]$ is non-zero.

B. Activity detection

Except $y_0[n]$ from the output of subband filter \mathcal{H}_0 corresponding to the subband associated with the system frequency F_0 , the outputs from the rest of subband filters are passed thorough activity detectors $(\mathcal{D}_e, \mathcal{D}_k)$ to determine the level of compression required, ranging from transmitting at the subband Nyquist rate to full compression that eliminates the transmission of $y_k[n]$.

The activity detection is performed on blocks of samples. The detector \mathcal{D}_k takes a block of samples and outputs an indicator $w_k = 1$ for the block if the subband k is active and $w_k = 0$ otherwise. The detector for inter-harmonic subband does the same way. A standard implementation of the activity detector is the energy detector whereas more sophisticated techniques such as quickest detection or machine-learning based detection can also be used.

C. Subband compression

The compression of the harmonic subband k is achieved by down-sampling of $y_k[n]$ by S_k fold. By the (passband) Nyquist sampling theorem, if the k th subband has passband bandwidth of W_k , then the signal in the k th subband can be perfectly reconstructed by sampling $x_k(t)$ at frequency of W_k (Hz). Given that $x(t)$ is sampled at F_s (Hz), the rate of down-sampling S_k is given by

$$S_k = \left\lceil \frac{F_s}{W_k} \right\rceil.$$

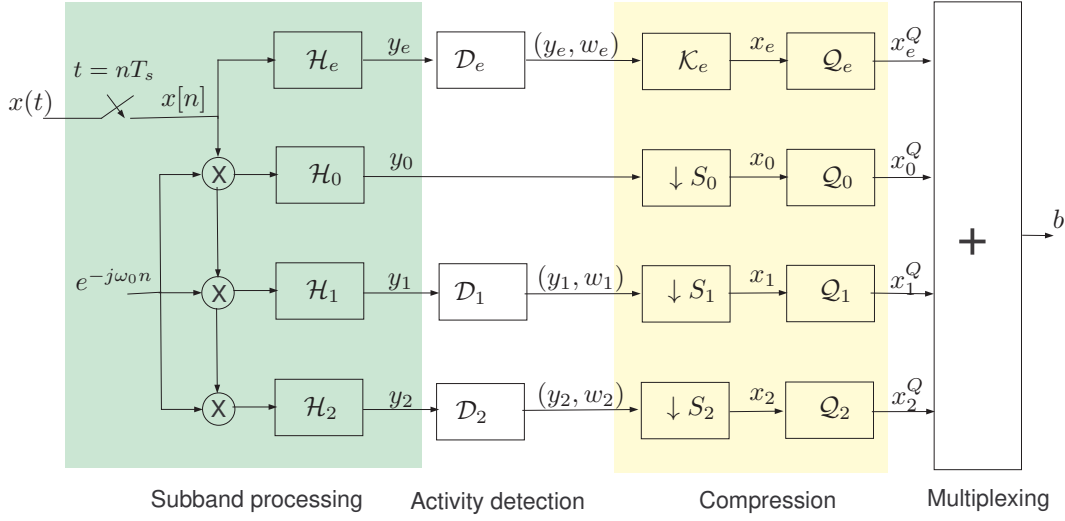


Fig. 3: A three-subband ASBC encoder where $h_k[n]$ is the impulse response of the k th subband filter. Time indices of signals are omitted with y_i standing for sequence $(y_i[n])$.

If subband k is active, the down-sampler gives the compressed data sequence

$$x_k[n] = \begin{cases} y_k[n], & n \equiv 0(\text{mod } S_k) \text{ and } w_k[n] = 1, \\ \sharp, & \text{otherwise,} \end{cases} \quad (3)$$

where \sharp is a masking symbol indicating that the data sample needs not be encoded and transmitted. Note that, although we define $x[n]$ for all n , only unmasked data blocks are transmitted over the network. The data rate associated with $x_k[n]$ is at most $1/S_k$ of that of $y_k[n]$.

The interharmonic band is expected to be active infrequently. When an interharmonic signal needs to be transmitted to the control center, an FFT-based (e.g., FFT- (k, L)) described in Sec. V-B) or wavelet based compression scheme can be used. See references in [4].

D. Quantization and multiplexing

The down-sampled data streams are quantized by quantizer (Q_e, Q_k) that maps subband stream $x_k[n]$ into a bit-stream \hat{x}_k^Q . A scalar quantizer, such as pulse-code modulation (PCM), differential PCM (ADPCM), and Sigma-Delta modulation, maps $x_k[n]$ when $n \equiv 0(\text{mod } S_k)$ into B_k bits. A vector quantization scheme [18], such as code excited linear prediction (CELP) or K -mean clustering, takes a block of M_k samples and map it to $M_k B_k$ bits. The bit-streams from subbands are multiplexed into a single bit-stream b to be delivered to the receiver. Also communicated are the sequence of activity indicators \sharp , one for each block that are not transmitted due to inactivity.

IV. ADAPTIVE SUBBAND COMPRESSION: DECODER

The ASBC decoder is located at the regional phasor data concentrator (PDC) or control center where compressed streaming data are reconstructed. Fig. 4 illustrates

the schematic of an ASBC decoder. The functionalities of individual components are explained below.

The de-multiplexing block is the inverse of the multiplexing block at the encoder. It parses the single bit-stream into subband data streams x_k^Q and x_e^Q sent by the transmitter.

The decompression block reverses the compression block and generates estimated harmonics (in baseband) \hat{y}_k in two steps. First, $x_k^Q[n]$ is up-sampled (interpolated) with zeros (including replacing masked symbols with zeros) to generate sequence $u_k[n]$ that has the same data rate as that of $y_k[n]$. The interpolated sequence $u_k[n]$ is passed through a subband interpolation filter \mathcal{H}^\dagger with impulse response $\hat{h}_k[n]$ to produce an estimate of the baseband representation of the k th harmonic signal $y_k[n]$. The subband interpolation filter may be chosen as the matched-filter $\hat{h}_k[n] = h_k[-n]$ to maximize the signal-to-noise ratio. Other implementations such as windowed low-pass filters can also be used. The decompression of the interharmonic signal follows directly the decompression algorithm used at the encoder.

The final decompression step takes the subband signals $\hat{y}_k[n]$ produce an estimate of the original direct sampled $x[n]$ of $x(t)$ in the encoder:

$$\hat{x}[n] = \sqrt{2}\text{Re}\left(\sum_{k=0}^K \hat{y}_k[n] e^{jk\omega_0 n}\right) + \hat{y}_e[n].$$

V. RATE-DISTORTION CHARACTERISTICS

The standard measure of lossy compression is the rate-distortion curve that highlights the tradeoff between the level of compression and the accuracy of the reconstruction. In general, a well designed compression scheme should have a monotonic rate-distortion curve: the higher the rate of the compressed signal, the lower the distortion.

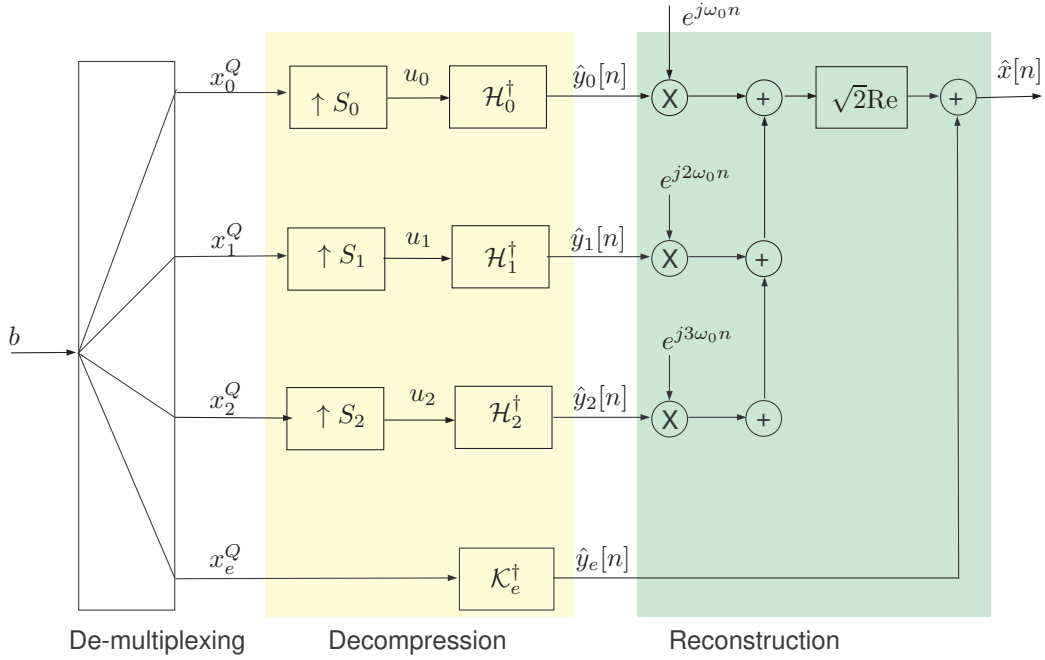


Fig. 4: A three-subband ASBC decoder. Time indices of internal signals (x_i^Q, u_i) are omitted.

In this paper, we adopt the compression ratio and the normalized mean-squared error to characterize the rate-distortion characteristics. Given a compression scheme χ , its *compression ratio* defined by

$$\eta^\chi = \frac{R^{\text{uc}}}{R^\chi},$$

where R^{uc} is the data rate (bits/sec) of the uncompressed signal and R^χ the rate of the compressed stream.

Let $x[n]$ be the original (uncompressed) signal and $\hat{x}^\chi[n]$ the reconstructed signal at the decoder. The *normalized mean-squared error (NMSE)* in (dB) is defined by

$$\begin{aligned} \mathcal{E}^\chi &= 10 \log_{10} \frac{\sum_{n=1}^N |x[n] - \hat{x}^\chi[n]|^2}{\sum_{n=1}^N x^2[n]} \quad (\text{dB}) \\ &\rightarrow 10 \log_{10} \frac{\mathbb{E}(|x[n] - \hat{x}^\chi[n]|^2)}{\mathbb{E}(|x[n]|^2)} = (\text{SNR}^\chi)^{-1} \quad (4) \end{aligned}$$

where N is the length of the data sequence, and the mean-square convergence of (4) assumes regularity conditions. Note that $\frac{1}{\mathcal{E}^\chi}$ has the interpretation to be the signal-to-reconstruction noise ratio (SNR).

For the application at hand, the data rate of the uncompressed data stream can be measured by

$$R^{\text{uc}} = F_s R_Q \quad (\text{bits/sec})$$

where F_s represents the sampling frequency of the measured signal $x(t)$ and R_Q the rate of quantization (bits/sample). The distortion of the uncompressed scheme comes only from

quantization error. For the simple R_Q bits PCM quantization, the NMSE is approximately by

$$\mathcal{E}^{\text{uc}} \approx -6R_Q + 1.25 \quad (\text{dB}).$$

See [19, p. 197].

A. Rate-distortion measure of ASBC: ($\eta^{\text{ASBC}}, \mathcal{E}^{\text{ASBC}}$)

We provide a characterization of the compression ratio η^{ASBC} and the NMSE of the reconstruction $\mathcal{E}^{\text{ASBC}}$, assuming that ASBC uses the same sample-by-sample quantization (R_Q bits/sample) as in the uncompressed scheme.

The data rate of the compressed data stream by ASBC is then given by

$$R^{\text{ASBC}} = F_s R_Q \sum_{k=0}^K p_k \frac{R_k}{S_k} + p_e R_e \quad (\text{bits/sec}), \quad (5)$$

where F_s is the sampling frequency of the uncompressed data, p_k the probability of k th subband being active, R_k the quantization for the k th subband, S_k the down-sampling rate of k th subband, p_e the probability that the interharmonic subband is active, and R_e the rate of compressed interharmonic subband. The compression ratio of ASBC is given by

$$\eta^{\text{ASBC}} = \frac{R^{\text{uc}}}{R^{\text{ASBC}}} = \left(\sum_{k=0}^K p_k \frac{R_k}{R_0 M_k} + p_e \frac{R_e}{F_s R_Q} \right)^{-1}.$$

The NMSE measure $\mathcal{E}^{\text{ASBC}}$ of ASBC depends on how accurately ASBC can detect the activities of harmonic and interharmonic subbands. Assuming all harmonic subbands are

active and there is no interharmonics, *i.e.*, $p_e = 0$, we have $\mathcal{E}^{\text{ASBC}} \approx \mathcal{E}^{\text{uc}}$ because ASBC achieves perfect reconstruction of each harmonic signals by the Nyquist sampling theorem. In practice, $\mathcal{E}^{\text{ASBC}} > \mathcal{E}^{\text{uc}}$ when false negative detection occurs or when there is interharmonic signal.

B. Rate-distortion measure of FFT-(k, L) : ($\eta^{\text{FFT}}, \mathcal{E}^{\text{FFT}}$)

A benchmark compression scheme is based on the fast Fourier transform (FFT), herein referred to as FFT-(k, L). It takes a block of L data samples, computes the FFT coefficients, and keeps only the k largest coefficients (corresponding to the positive frequencies) and masks the rest.

The compression ratio of FFT-(k, L) is given by

$$\eta^{\text{FFT}-(k, L)} = \frac{L}{2k}$$

where we ignore the $\log_2 L$ bits needed to encode the frequency locations[§]. The NMSE of FFT-(k, L) is given by

$$\mathcal{E}^{\text{FFT}-(k, L)} = 10 \log \left(1 - \frac{\sum_{i=1}^{2k} |X_{(i)}|^2}{\sum_{i=1}^N |x[i]|^2} \right)$$

where $X_{(i)}$ is the discrete Fourier coefficients with the i th largest magnitude in the L -block FFT.

VI. NUMERICAL RESULTS

We present in this section numerical results in three categories. The first category is a comparison study using a set of synthetic waveforms having characteristics of power system signals. Such tests allow us to evaluate the performance of benchmark techniques under different scenarios of transient events. The second category is the compression of real data obtained by direct sampling of voltage measurements at 6 kHz. This is a case that the signal has significant harmonics and interharmonics. The third category is the compression of compression techniques on streaming of PMU frequency measurements.

The three benchmark techniques compared in this study were (i) FFT described in Sec. V-B, (ii) Multi-resolution discrete wavelet transform (DWT) [20], and (iii) ASBC developed in this paper. All three methods were implemented based on a 0.5-second data block. We measured the performance of compression by the rate-distortion curve by plotting the NMSE (dB) against the compression ratio η . The maximum reconstruction error measure was also used.

Note that the rate-distortion curves typically slope downward: the greater the η^{-1} , the lower the compression ratio (the higher the data rate of the compressed data stream), the lower the reconstruction error.

[§]Note that the factor 2 in the denominator accounts for the fact that FFT coefficients are in general complex and anti-symmetrical for real $x[n]$.

TABLE I: Test waveforms.

Test cases	Signal waveforms
Normal state: $\sigma_t = 0$	$x_N(t) = \sum_{k=0}^K a_k \cos(2\pi 60(k+1)t + \phi_k)$
Event: $\sigma_t = 1$	$x^{\text{AM}}(t) = \alpha_0 + \alpha \cos(2\pi \Delta t) \cos(2\pi 60t + \theta_0)$ $x^{\text{FM}}(t) = \alpha \cos(2\pi 60t + \beta \cos(2\pi \Delta t - \pi) + \theta_0)$ $x^{\text{Chirp}}(t) = \alpha \cos(2\pi(59.5 + \gamma t) + \theta_0)$ $x^{\text{IH}}(t) = \sum_{k=1}^W \alpha_k \cos(2\pi f_k t + \theta_k)$

Signal parameters: σ_t —the switching state, (a_k, ϕ_k) —amplitude and phase angles of harmonics, $(\alpha_k, \beta, \gamma, \theta_k)$ —transient parameters, and f_k —interharmonic frequencies.

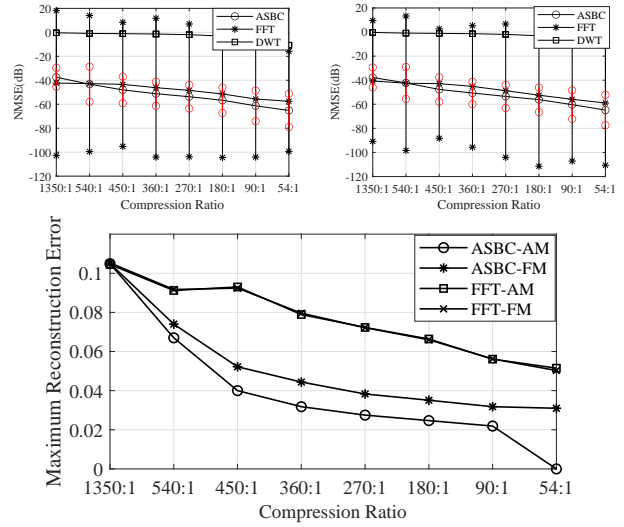


Fig. 5: FM/AM parameters: $\alpha_0 = 1, \lambda = 0.1, \mu = 2$. Top panel NMSE with 95% confidence interval for the AM (Left) and FM (right) events. No high order harmonics and interharmonics. Bottom: the maximum reconstruction error for the FM and AM events.

A. Compression of synthetic waveforms

The purpose of this experiment was to test the performance of compression when the regular sinusoidal waveform was interrupted by episodes of transient events with signals of different characteristics. We focused on four types of event signals shown in Table I. Among the set of waveforms at the event state, the amplitude modulation (AM) and frequency modulation (FM) waveforms were designed according to the requirement on performance under dynamic compliance specified by [3]. The linear chirp waveform was used to simulate the frequency ramping events, and the interharmonic (IH) waveform modeled frequency components that were not multiples of system frequency F_0 .

To simulate transient events, we used a two-state Markov switching model that modulated the signal between the normal state ($\sigma_t = 0$) waveform $x^{\text{Norm}}(t)$ and the event state ($\sigma = 1$) with waveforms chosen from AM, FM, chirp, and IH signals. The Markov switching process was characterized

by state transition rate (λ, μ) where $1/\lambda$ was the expected holding time of the normal state and $1/\mu$ the expected holding time of the event state.

Fig. 5 shows the rate-distortion curve of ASBC, FFT, and DWT techniques for the FM and AM events. The sampling rate of the original signal was at 5400 Hz. As shown in the upper panel, the NMSE of DWT scheme was about 30 to 40 dB higher than those of FFT and ASBC. ASBC had about 4-6 dB gain over FFT for the compression ratio between 540:1 and 54:1 whereas FFT had 3 dB gain at compression ratio of 1350:1. Note that the 95% confidence interval of ASBC was considerably smaller than that of FFT, indicating that the errors of FFT scheme were more dispersed. The same behavior was confirmed by the maximum reconstruction error plot at the lower panel of Fig. 5. DWT, on the other hand, had a much narrower confidence interval (thus not shown on the plot). The main reason that ASBC outperformed FFT was that FFT introduced discontinuities at the boundaries of FFT blocks. In contrast, ASBC encoder did not have discontinuities. This phenomenon was more pronounced for the linear-chirp test cases shown in Fig. 6

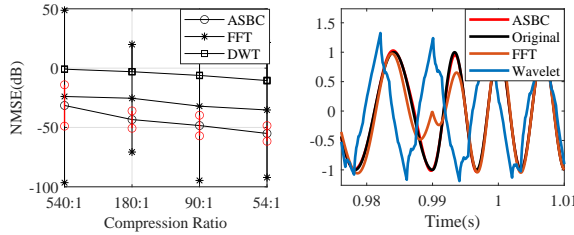


Fig. 6: Left: comparison of rate-distortion curve for linear chirp events. Right: a segment of the original and its reconstruction. $\lambda = 0.1$, $\mu = 1$

Fig. 6 shows the rate-distortion plot for the linear chirp events. The linear chirp signals have a much wider bandwidth and the achievable compression ratio significantly lower than the FM/AM events. The left panel shows the NMSE for the three techniques. Again, DWT was not competitive against FFT and ASBC techniques, and ASBC had considerable gain over FFT in the low compression ratio regime. In particular, ASBC had about 15 dB lower NMSE at the compression ratio of 180:1 and 20 dB lower at the compression ratio of 54:1. The right panel shows the original signal and reconstructed ones in the time domain. Notice the transition of the normal sinusoidal waveform transitioned to a linear chirp at time $t = 0.99$ second. The reconstruction of FFT around $t = 0.99$ showed significantly larger error than that of ASBC.

B. Compression of Direct Voltage Measurements.

We applied ASBC directly to a data set (henceforth referred to as UTK6K) provided by the University of Tennessee, Knoxville. The UTK6K data set consisted of 1.8 million voltage measurements sampled at 6KHz. Fig. 7

(Top) shows the power spectrum of the directly sampled data stream, from which we observed the presence of harmonics and interharmonics. The plot also showed that the energy levels from the 20th to 50th subbands were negligible.

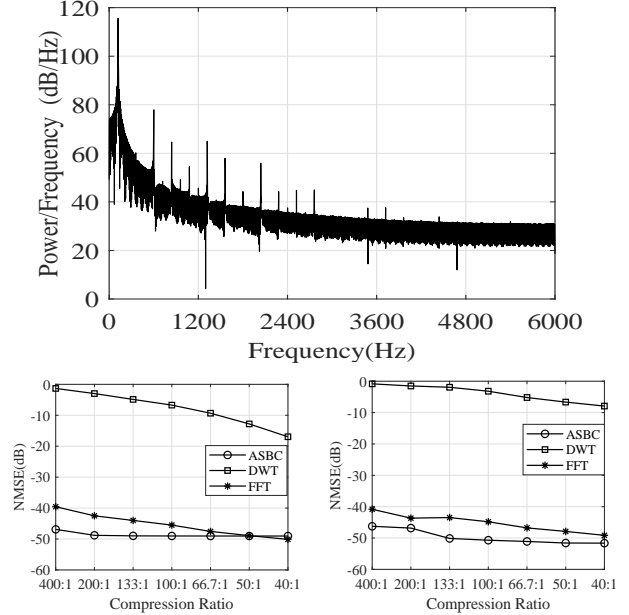


Fig. 7: Top: Power spectrum density of the direct voltage measurements. Bottom left: comparison of rate-distortion curves without interharmonics. Bottom right: comparison with added interharmonics.

ASBC was implemented with 3 Hz bandwidth for all subbands associated with all 50 harmonics, and only the top k subbands that have the highest energy level were compressed and delivered where k was chosen to have required compression ratio. The bottom left panel of Fig. 7 shows the rate-distortion curve of ASBC, FFT and DWT for the compression ratio from 400:1 to 40:1. For this range of compression ratio, DWT was not competitive. ASBC was seen to out-perform FFT in the compression ratio range of 400:1 to 100:1, and the two schemes are comparable for the range of 66.7:1 to 40:1. The reason that FFT-based compression did not perform well was, again, that the block implementation of FFT introduced discontinuities, which caused reconstruction errors. As the compression ratio decreased, more FFT coefficients were preserved, the reconstruction error of FFT improved.

To evaluate the effects of interharmonics, we added additional interharmonic transient events to the original UTK6KHz dataset in the same way as experiments discussed in Sec. VI-A. The bottom right panel of Fig. 7 shows the rate distortion plot with interharmonics subband activated. An energy detector was used to determine when and whether the interharmonics subband should be activated. Only those harmonics subbands with sufficient energy level were compressed and transmitted. Interharmonics subband, when de-

tected being active by the energy detector, was compressed dynamically to the effective bandwidth ranging from 60 to 120Hz. Comparing with the rate-distortion performance on the bottom left panel, The presence of interharmonics increased NMSE slightly for ASBC at the high compression ratio. Overall, ASBC consistently performed better than other methods. The standard deviations was small for all three methods, thus the confidence intervals were not shown in the plot.

C. Compression of PMU data

We applied ASBC to a dataset referred to as UTK1.44, which consisted of frequency estimates from the University of Tennessee, Knoxville. The dataset contained two data streams, each with 1,800,000 samples at the sampling rate of 1.44 kHz. One distinct feature of this dataset was the frequency ramping event during [308.4 – 308.6] sec as shown in the lower panel of Fig. 8. For this application, the frequency measurements were expected to be centered around 60 (Hz). As a time series, the frequency measurements are close to be constant. Thus only a single subband is needed for ASBC. We varied the subband bandwidth to achieve different compression ratios.

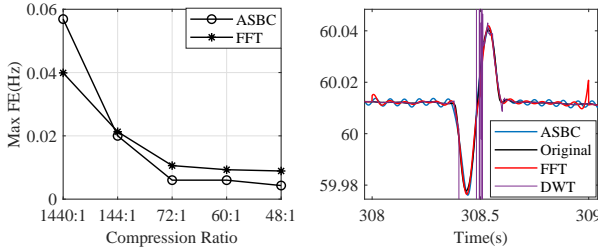


Fig. 8: Maximum FE and time-domain reconstruction

The performance of the three data compression method was evaluated base on the maximum error of the reconstruction of the frequency measurements (Max FE) as defined by the IEEE Standard C37.11 [3] that specified the acceptable performance is to have Max-FE below 0.005 Hz. The left panel of Fig. 8 shows the Max-FE against compression ratio. Max-FE for DWT was always larger than 80, thus is not shown in the plot. In this case, ASBC and FFT appeared to have similar performance along the rate-distortion curve, both having Max-FE below 0.005 for compression ratios lower than 72:1, within which ASBC performed slightly better. The right panel of Fig. 8 showed the time-domain reconstructions at the compression ratio of 48:1. Note that the small spike of reconstruction error of FFT at round $t = 309$ sec caused by, again, the discontinuity of the block implementation of FFT.

VII. CONCLUSION

We have developed an adaptive subband compression (ASBC) technique for the streaming of measurement data

of a wide-area measurement system. Different from existing technologies, ASBC employs a filter-bank that decomposes measurements based on the harmonic structure of the signal waveforms and adaptively compresses individual harmonic components. A prototype implementation of ASBC offers a significantly improved rate-distortion tradeoff.

REFERENCES

- [1] Y. Liu, "Beyond today's synchrophasor," in *NSF Workshop on Forging Connections between Machine Learning, Data Science, and Power Systems Research*, March 2020, [ONLINE], available (2020/8/20) at <https://sites.google.com/umn.edu/ml-ds4pes/presentations>.
- [2] IEEE, "IEEE standard for interconnection and interoperability of distributed energy resources with associated electric power systems interfaces," *IEEE Std 1547-2018 (Revision of IEEE Std 1547-2003)*, pp. 1–138, April 2018.
- [3] —, "IEEE standard for synchrophasor data transfer for power systems," *IEEE Std C37.118.2-2011 (Revision of IEEE Std C37.118-2005)*, pp. 1–53, Dec 2011.
- [4] M. P. Tcheu et al., "The compression of electric signal waveforms for smart grids: State of the art and future trends," *IEEE Transactions on Smart Grid*, vol. 5, no. 1, pp. 291–302, Jan 2014.
- [5] C. E. Shannon, "A mathematical theory of communication," *Bell Sys. Tech. Journal*, vol. 27, pp. 379–423, 623–656, 1948.
- [6] K. Mehta and B. D. Russell, "Data compression for digital data from power systems disturbances: requirements and technique evaluation," *IEEE Transactions on Power Delivery*, vol. 4, pp. 1683–1688, 1989.
- [7] T. Cover and J. Thomas, *Elements of Information Theory*. John Wiley & Sons, Inc., 1991.
- [8] T. B. Littler and D. J. Morrow, "Wavelets for the analysis and compression of power system disturbances," *IEEE Transactions on Power Delivery*, vol. 14, no. 2, pp. 358–364, April 1999.
- [9] S. Santoso, E. J. Powers, and W. M. Grady, "Power quality disturbance data compression using wavelet transform methods," *IEEE Transactions on Power Delivery*, vol. 12, no. 3, pp. 1250–1257, July 1997.
- [10] A. M. Gaouda, M. M. A. Salama, M. R. Sultan, and A. Y. Chikhani, "Application of multiresolution signal decomposition for monitoring short-duration variations in distribution systems," *IEEE Transactions on Power Delivery*, vol. 15, no. 2, pp. 478–485, April 2000.
- [11] S. Santoso, E. J. Powers, W. M. Grady, and A. C. Parsons, "Power quality disturbance waveform recognition using wavelet-based neural classifier. i. theoretical foundation," *IEEE Transactions on Power Delivery*, vol. 15, no. 1, pp. 222–228, Jan 2000.
- [12] P. K. Dash, B. K. Panigrahi, D. K. Sahoo, and G. Panda, "Power quality disturbance data compression, detection, and classification using integrated spline wavelet and s-transform," *IEEE Transactions on Power Delivery*, vol. 18, no. 2, pp. 595–600, April 2003.
- [13] N. Tse et al., "Real-time power-quality monitoring with hybrid sinusoidal and lifting wavelet compression algorithm," *IEEE Transactions on Power Delivery*, vol. 27, no. 4, pp. 1718–1726, Oct 2012.
- [14] S. Meher, A. Pradhan, and G. Panda, "An integrated data compression scheme for power quality events using spline wavelet and neural network," *Electric Power Systems Research*, vol. 69, pp. 213–220, 2004.
- [15] W. R. A. Ibrahim and M. M. Morcos, "Novel data compression technique for power waveforms using adaptive fuzzy logic," *IEEE Transactions on Power Delivery*, vol. 20, no. 3, pp. 2136–2143, 2005.
- [16] Y. Ge, A. J. Flueck, D. Kim, J. Ahn, J. Lee, and D. Kwon, "Power system real-time event detection and associated data archival reduction based on synchrophasors," *IEEE Transactions on Smart Grid*, vol. 6, no. 4, pp. 2088–2097, July 2015.
- [17] A. Testa et al., "Interharmonics: Theory and modeling," *IEEE Transactions on Power Delivery*, vol. 22, no. 4, pp. 2335–2348, 2007.
- [18] A. Gersho and R. M. Gray, *Vector Quantization and Signal Compression*. USA: Kluwer Academic Publishers, 1991.
- [19] A. V. Oppenheim and R. W. Schaffer, *Discrete-Time Signal Processing*, 2nd ed. USA: Prentice Hall Press, 1999.
- [20] J. Ning, J. Wang, W. Gao, and C. Liu, "A wavelet-based data compression technique for smart grid," *IEEE Transactions on Smart Grid*, vol. 2, no. 1, pp. 212–218, March 2011.

Adaptive Subband Compression of Streaming Data for Power System Monitoring and Control

Xinyi Wang and

Abstract—A data compression system capable of providing high fidelity streaming of power system measurements at low bandwidth is presented. Referred to as adaptive subband compression (ASBC), the proposed technique partitions signal into harmonic subbands and adaptively compresses subband signals based on the level of activities within each subband. ASBC conforms to existing industry standards for phasor measurement units (PMU) and applies to techniques involving high-frequency sampling of power system signals. Experiments on actual phasor measurement data and standard test cases show that the prototyped technology reduces the required communication data rate by several orders of magnitude while maintaining the precision required by industry standards.

Index Terms—Phasor measurement unit (PMU), power system monitoring and control, subband coding, adaptive data compression.

I. INTRODUCTION

A. Background

Modern power systems are large complex dynamical systems whose behavior defies simple mathematical characterizations. A minor event such as tripping of a transmission line or the loss of a generator can drive the system along a trajectory that appears normal for an extended period and suddenly bifurcates to oscillations, chaotic motions, and an abrupt collapse. Some of the well-known examples are the August 1982 large area voltage collapse in the Belgian system [1] and the 2003 northeast blackout in the U.S. [2]. Minor outages are increasingly more common as greater integration of intermittent renewable sources such as wind and solar power.

What makes this problem especially difficult is that the process of blackout is a combination of cascading and voltage collapse dynamics [3]. Understanding and predicting voltage collapse are long-standing open problems whose solutions have eluded decades of extensive efforts [4], [5].

A promising line of approaches is based on *data analytic*, machine learning (ML), and artificial intelligence (AI) solutions that incorporate streaming data from a wide-area monitoring system (WAMS) that provides real-time situational awareness. By extracting hidden signatures from measurement data and exploiting structural properties of the underlying physical model, such solutions have the potential

to allow the system operator to take remedial actions before the commencing cascading blackout.

A prerequisite of modern data analytic, ML, and AI solutions is the ability to observe the system state at the millisecond timescale commensurate with the fast transient dynamics. To this end, the invention of the phasor measurement unit (PMU) technology in the late '80s was considered a major engineering breakthrough in power systems [6]–[8]. Through globally synchronized phasor and frequency measurements communicated at the rate of 60 to 120 measurements per second to the control center, the PMU technology has the potential to revolutionize power system operations by providing the essential signal intelligence for fast timescale security monitoring and enhanced network resilience [9]–[14]. Indeed, monitoring transient and voltage instability at a fast-timescale has always been considered as one of the killer applications of PMU [15]–[21].

Despite over billion-dollar investments by governments and industries worldwide, however, PMU technology so far has not realized the anticipated benefits. A significant cause of under-achievement is twofold. First, for the technology to be effective, PMUs need to be broadly deployed. Unfortunately, the cumulative installation of PMU remains limited, sufficient for some high voltage networks, but grossly inadequate for large systems. The deployment of PMU in the distribution systems is barely noticeable. Apparently, PMU adoption has fallen in the classical chicken-and-egg trap; the lack of deployment limits the capabilities of the technology, and the lack of demonstrated capabilities inhibits the necessary infrastructure investment for broader deployments.

Second, there are technical barriers that PMU must overcome to be effective as the key technology for real-time monitoring and control of a large power grid. The current reporting rate at up to 240 frames per second does not capture fast transients and high-order harmonics in the power system. With greater penetration of renewable energy, the increasing presence of power electronics associated with wind, solar, and distributed generation introduces substantial high-order harmonics [22], [23, p. 99]. The IEEE Standards for Interconnection and Interoperability of Distributed Energy Resources [24] and Synchronphasor Measurements [25] both set the requirement for current harmonics distortion up to 50th order. The signal bandwidth can be significantly higher during transient events at times of significant contingencies. By the Shannon-Nyquist theorem, direct sampling of signals

of such bandwidth requires 6 kHz sampling rate to achieve the high fidelity reconstruction of the original signal. Such a sampling rate is approximately 50-100 times faster than that specified by the current industry standard [25]. If the PMU technology is to be a key technology for monitoring the fast dynamics of a power system, it needs the capability to produce synchronized measurements at a significantly higher resolution than that required by the current standard. More importantly, communicating such high resolution and high fidelity measurements must not exceed the capability of the existing communication infrastructure.

B. Summary of Results

We propose a lossy compression technique for data streaming of measurements from a wide area monitoring system (WAMS) that enables high-fidelity and high-resolution PMU technology without requiring upgrades of the existing data collection, communication, and networking infrastructure. At the core of the technology is an adaptive lossy compression technique, referred to as *adaptive subband compression* (ASBC) that provides a 100:1 to 1000:1 compression ratio. The implication is that, under the 10 Hz reporting rate of the existing PMU technology, measurements sampled at the equivalent of 1K-10K Hz can be communicated to data concentrators or the control center.

ASBC consists of an ASBC encoder for each remote sensing device, and an ASBC decoder at the fusion center*. Together, they form the ASBC codec that provides an end-to-end data streaming at 1-30 kHz per-channel high-resolution voltage and current measurements. Fig. 1 illustrates a conceptual realization of the ASBC technology.

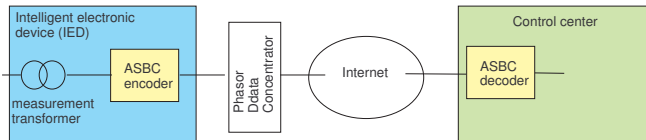


Fig. 1: An application of ASBC technology for high resolution PMU monitoring of power grids.

The ASBC encoder includes the following components:

- 1) a filterbank that decomposes voltage and current measurements into subband signals associated with different harmonics,
- 2) a detector for each subband signal that detects novel activities related to a particular harmonic,
- 3) a variable-rate down-sampling technique for the subband signals, and
- 4) a variable-rate quantization technique for the sampled subband signal.

A schematic of the ASBC encoder is shown in Fig. 3.

*A fusion center is the location where data streams from different sensing devices are combined. A fusion center may be located at PMU data concentrators (PDC) or the operator's control center.

The ASBC decoder includes the following components:

- 1) a variable rate upsampling of each subband data stream,
- 2) an interpolation filterbank that creates high-resolution baseband data streams, and
- 3) a synthesizer that combines subband data streams into a reproduction of the original data sequence.

A schematic of the ASBC encoder is shown in Fig. 4.

C. Summary of Related Work

The need for data compression for power system monitoring goes back at least three decades. Mehta and Russell made one of the earliest contributions in [26], where the authors articulated the need for data compression due to limited capacity of communications.

Mehta and Russell recommended two techniques that are particularly relevant to ASBC. One is to compress data in the frequency domain by the Fast Fourier Transform (FFT) and discard high-frequency coefficients. ASBC, too, compresses data in the frequency domain, although the implementation is subband filtering in the time domain. ASBC does not discard high-frequency components; it eliminates only the out-of-the-band frequencies while keeping all frequency components around higher-order harmonics. The second technique recommended by Mehta and Russell is adaptive-differential pulse code modulation (ADPCM). ASBC employs PCM or ADPCM in quantizing the outputs of the subband filters.

There is an expansive literature in data compression for power quality data at digital fault recorders (DFR) [27]–[32]. For such applications, the data sampling rate can be as high as 10MHz, and the requirement for compression is different from that for real-time monitoring and control targeted by ASBC. In particular, because the recorded data are only uploaded on-demand, often in the events of failure or significant disturbances, the data must be preserved at high accuracy. Thus lossless compression techniques such as are often preferred. For continuous real-time monitoring, lossless compression is unnecessary, and it is best to adjust the compression rate adaptively. In addition, compression of this type of archival data does not have the requirement for real-time streaming data where the latency of compression and decompression is of major concern. Block processing techniques such as transforms (FFT and discrete-cosine transform (DCT), wavelet-spline) [26], [31], neural network and fuzzy logic [30], [33], [34], and principal component analysis (PCA) [35] are appropriate.

Data compression for real-time monitoring and control has a relatively short history. See a comprehensive survey on compression techniques for the smart grid [36], where the authors reported the capabilities of various compression techniques with compression ratio ranging from 2 to 5:1 for lossless compressions. Most relevant to this work are the lossy compressions, categorized by wavelet (and waveform packet) transform techniques, mixed transform, and parametric compression techniques. These state-of-the-art offers a 6

to 16:1 compression ratio at the normalized mean squared error (NMSE) of from minus 20 to 30 dB. As a lossy compression technique, the subband coding solution ASBC proposed here does not fit in the general categories of existing solutions. Comparing to current technologies, ASBC offers an improved compression ratio of 400:1 at minus 39dB NMSE for some of the real voltage and PMU measurements and 100:1 at minus 25 to 52 dB NMSE for short duration AM-modulated signal.

II. SIGNAL MODEL

We model the continuous-time voltage (or current) signal $x(t)$ and its Fourier spectrum $X(f)$ by

$$x(t) = \sum_{k=0}^K x_k(t) \xleftrightarrow{\text{FT}} X(f) = \sum_{k=0}^K X_k(f), \quad (1a)$$

$$x_k(t) = a_k(t) \cos(k\Omega_0 t + \phi_k(t)) \xleftrightarrow{\text{FT}} X_k(f), \quad (1b)$$

where $\Omega_0 = 2\pi F_0$ and F_0 (Hz) is the nominal operating frequency (e.g., 50 or 60 Hz), $x_0(t)$ the voltage signal associated with the nominal frequency F_0 , and $x_k(t)$ the distortion associated the k th harmonic at kF_0 (Hz).

The spectrum $X(f)$ of $x(t)$ is illustrated in Fig. 2. We assume that the spectrum $X_k(f)$ of the k th harmonic is centered around $(k+1)F_0$ with passband bandwidth[†] of $W_k < F_0$. The bandwidth of $x(t)$ is therefore $KF_0 + \frac{W_K + W_0}{2}$.

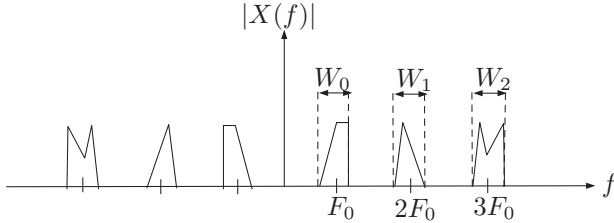


Fig. 2: The spectrum of $x(t)$ and its harmonics.

Sampled at the frequency of $F_s = \frac{1}{T_s}$ (Hz), the discrete-time signal is given by

$$x[n] := x(nT_s) = \sum_{k=0}^K x_k[n], n = 0, \pm 1, \pm 2, \dots \quad (2a)$$

$$x_k[n] := a_k[n] \cos(k\omega_0 n + \phi_k[n]). \quad (2b)$$

where $\omega_0 = \frac{\Omega_0}{F_s}$ and $a_k[n]$, $\phi_k[n]$ the sampled amplitude and phase angles associated with the k th harmonic. Let $X(\omega) = \sum_n x[n]e^{-j\omega n}$ be the discrete-time Fourier transform (DTFT) of $x[n]$.

[†]The passband bandwidth is defined by the width of the frequency band containing non zero frequency components.

III. ADAPTIVE SUBBAND COMPRESSION: ENCODER

ASBC encoder is part of the remote sensing partitions the signal spectrum into a set of frequency bands (channels), adaptively masks inactive bands, and encodes the unmasked bands separately. Fig. 3 illustrates the ASBC encoder at the remote sensing unit (PMU or IED). The functionalities of individual components are explained below.

A. Subband decomposition

From the output of the sensor transformer, the measured continuous-time signal $x(t)$ is sampled at F_s Hz. The discrete-time signal $x[n]$ is frequency-down shifted and pass through a filterbank with transfer function $H(z) = (H_0(z), \dots, H_K(z))$. The output of the filterbank is an $(K+1)$ dimensional complex time series $y[n] = (y_0[n], \dots, y_K[n])$. The output of the k th subband filter is given by

$$y_k[n] = (x[n]e^{-jk\omega_0 n}) \otimes h_k[n],$$

where \otimes is the convolution operator and $h_k[\cdot] \xleftrightarrow{\mathcal{Z}} H_k(z)$ the impulse response of the k th subband filter. Signal $y_k[n]$ is the baseband representation of the k th harmonic signal $x_k[n]$, and its continuous-time counter part is $\tilde{x}_k(t) = x_k(t)e^{-jk\Omega_0 t}$. In absence of high order harmonics, $x(t) = x_0(t)$ in (1), and only $y_0[n]$ is non-zero.

B. Activity detection

Except $y_0[n]$ from the output of subband filter H_0 corresponding to the subband associated with F_0 , the output $y_k[n]$ of subband filter $H_k(z)$ is passed through an activity detector \mathcal{D}_k to determine the level of compression for the signal component associated with the k th harmonic, ranging eliminating the data stream from compression to encoding it at the full Nyquist rate.

Detector \mathcal{D}_k can be implemented by an energy detector on a block-by-block basis. For a block of M_k data points starting at $n - M_k + 1$ and ending at n , let the empirical power level be

$$\hat{p}_k[n] = \begin{cases} \frac{1}{M_k} \sum_{m=0}^{M_k-1} |y_k[n-m]|^2, & n \equiv 0 \pmod{M_k} \\ \# & \text{otherwise} \end{cases},$$

where $\#$ stands for “no-value” that is to be ignored downstream. Detector \mathcal{D}_k compares $\hat{p}_k[n]$ with a threshold τ and produces a masking function for the data block

$$z_k[n] = \begin{cases} 1 & \text{if } \hat{p}_k[n] \geq \tau_k, n \equiv 0 \pmod{M_k} \\ 0 & \text{if } \hat{p}_k[n] < \tau_k \text{ and } n \equiv 0 \pmod{M_k} \end{cases}$$

$$z_k[n-i] = z_k[n] \text{ for } n \equiv 0 \pmod{M_k}, 0 \leq i < M_k.$$

The threshold τ_k is chosen to control the false positive rate when there is substantial energy in the k th harmonic while the detector \mathcal{D}_k declares otherwise.

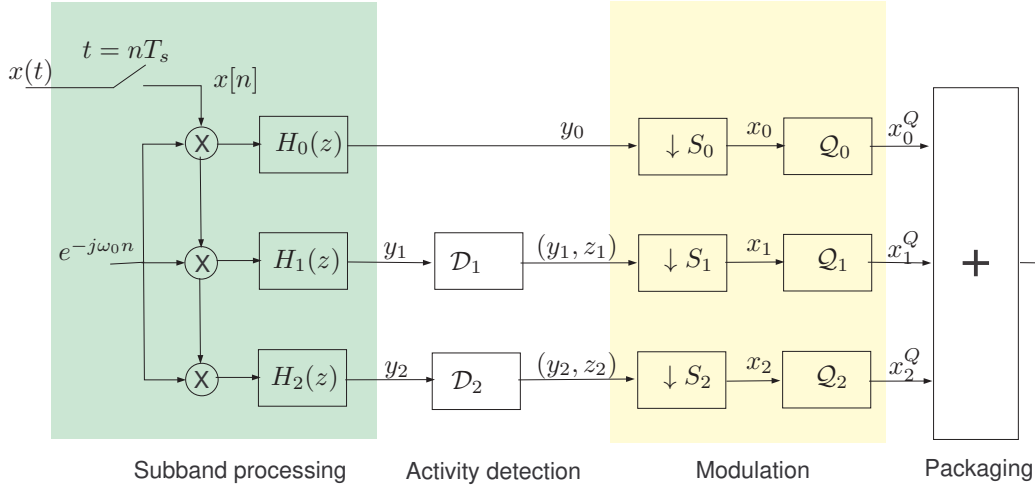


Fig. 3: A three-subband ASBC encoder. Time indices of internal signals are omitted with y_i standing for $y[n]$.

C. Modulation: down-sampling

In subband k , the outputs of the subband filter $y_k[n]$ and detector output $z_k[n]$ are input of a down-sampler that samples $y_k[n]$ one in every S_k data points, if detector \mathcal{D}_k indicates that the energy level in the data block is high. Specifically, the output of the down-sampler is given by

$$x_k[n] = \begin{cases} y_k[n], & n \equiv 0(\text{mod } S_k) \text{ and } z_k[n] = 1, \\ \#, & \text{otherwise,} \end{cases} \quad (3)$$

where no-value ($\#$) samples will not be encoded and transmitted downstream. Note that, although we define $x[n]$ for all n , only a fraction of $1/S_k$ data samples contain values to be transmitted to the receiver. Thus the data rate associated with $x_k[n]$ is $1/S_k$ of that of $y_k[n]$.

D. Modulation: quantization and packaging

Stripping the no-value ($\#$) data samples, the quantizer \mathcal{Q}_k maps $x_k[n]$ into a bit-stream \hat{x}_k^Q . A scalar quantizer, such as pulse-code modulation (PCM), differential PCM (DPCM), and Sigma-Delta modulation, maps $x_k[n]$ when $n \equiv 0(\text{mod } S_k)$ into B_k bits. A vector quantization scheme [37], such as code excited linear prediction (CELP) or K -mean clustering, takes a block of M_k samples and map it to $M_k B_k$ bits. The bit-streams from subbands are packaged into a single bit-stream b to be delivered to the receiver.

IV. ADAPTIVE SUBBAND COMPRESSION: DECODER

The ASBC decoder is located at the regional phasor data concentrator (PDC) or control center where PMU data are reconstructed (demodulated). Fig. 4 illustrates the schematic of an ASBC decoder. The functionalities of individual components are explained below.

A. Data parsing

The data parsing block parses the single bit-stream into subband data symbol streams \hat{x}_k^Q for associated with individual harmonics. The data stream \hat{x}_k^Q differs from x_k^Q in the encoder only because of the quantization errors introduced by \mathcal{Q}_k .

B. Demodulation

The demodulator takes parsed data sequence $\hat{x}_k^Q[n]$ and up-sample the data sequence by M_k fold to produce \hat{x}_k by inserting zeros at places of x_k where no-value ($\#$) symbols are located. Specifically, if we ignore the quantization error, $\hat{x}_k[n]$ are simply $x_k[n]$ with no-value ($\#$) symbols replaced by zeros.

The up-sampled data sequence $\hat{x}[n]$ are then passed through a subband filter $\hat{H}_k(z)$ to produce an estimate of the baseband representation of the k th harmonic signal $y_k[n]$. The interpolation filter may be chosen as the matched-filter that matches to $H_k(z)$ to enhance the signal-to-noise ratio. Other implementations such as the ideal low-pass filter are also admissible.

C. Decompression

The final decompression step takes the subband signals $\hat{y}_k[n]$ produce an estimate of the original direct sampled $x[n]$ of $x(t)$ in the encoder:

$$\hat{x}(t) = \text{Re} \left(\sum_k \hat{x}_k[n] e^{jk\omega_0 n} \right).$$

V. DIRECT PMU DATA COMPRESSION

The ASBC scheme presented above applies directly to the direct compression of phasor and frequency measurements. In such an application, the voltage/current phasor

and frequency estimates are produced locally by the remote sensors. Assuming that the phasor and frequency estimation algorithms already take into account higher-order harmonics, the problem of compression simplifies to a single-subband compression problem.

The encoder at the remote sensing device implements only the subband filter $H_0(z)$ without frequency downshift as shown in Fig 3. The output $y_0[n]$ of $H_0(z)$ is down sampled by S_k fold and quantized to x_0^Q and converted to a single-channel bit stream b . The decoder at the PDC or control center implements the top branch of the decoder in Fig 4.

VI. PARAMETER DESIGN AND PERFORMANCE

We discuss in this section choices of design parameters and performance of ASBC. For the encoder, we consider each subband separately. The parameters for the k th subband encoder that compresses the k th harmonic $x_k(t)$ are the down-sampling rate S_k and per-sample quantization rate B_k bits/sample. The two parameters can be chosen independently or jointly.

For the PCM quantization scheme, S_k should be such that $F_s/S_k \geq W_k$ where W_k is the bandwidth of $x_k(t)$. The quantization rate B_k should be such that the quantization error satisfies some prescribed error criterion. Let the total vector error (TVE) for complex measurement $x[n]$ be

$$\text{TVE} := \sqrt{\frac{|x^Q[n] - x[n]|^2}{|x[n]|^2}} \approx \frac{1}{\sqrt{\text{SNR}}}$$

where SNR is the signal-to-quantization noise ratio (SNR) of PCM. Measured in dB, we have

$$\text{TVE}_{\text{dB}} \approx -\text{SNR}_{\text{dB}}.$$

The SNR (in dB) for PCM with B_k bits is given by

$$\text{SNR}_{\text{dB}} = 1.76 + 6B_k.$$

Thus for the 1% TVE required by the IEEE STD C37.118.1, the number of bits required for PCM is given by

$$10 \log_{10} 0.01 \approx -1.76 - 6B_k \Rightarrow B_k \approx 3.04(\text{bits/sample})$$

Suppose that the bandwidth of the k th harmonics is W_k Hz, setting $S_k = F_s/W_k$, the average bit rate of the k th subband encoder is given by

$$R_k = W_k B_k \Pr(z_k[(n \bmod M_k)] = 1),$$

where $\Pr(z_k[(n \bmod M_k)] = 1)$ is the probability that a block of M_k data samples of the k th harmonic is detected to be active. As an example, if $W_k \approx 3$ (Hz), $B_k = 4$ bits/sample, and $\Pr(z_k[(n \bmod M_k)] = 1) = 1$, we have $R_k = 12$ bits/sec.

If total no higher order harmonics are present and under the 1% TVE requirement and signal bandwidth W_0 of 3Hz, the bit-rate of ASBC is given by

$$R^{\text{ASBC}} = W_0 B_0 \approx 12 \text{ (bits/sec)}.$$

In comparison, under the current frame rate of 120 Hz, the PMU measurement (without higher order harmonics) using the same PCM quantization is 480 (bits/sec). Thus ASBC achieves approximately compression ratio of 40. This means that, under the same 120 Hz framerate used under the current standard, ASBC enables communication of measurements that include up to 39 active harmonics.

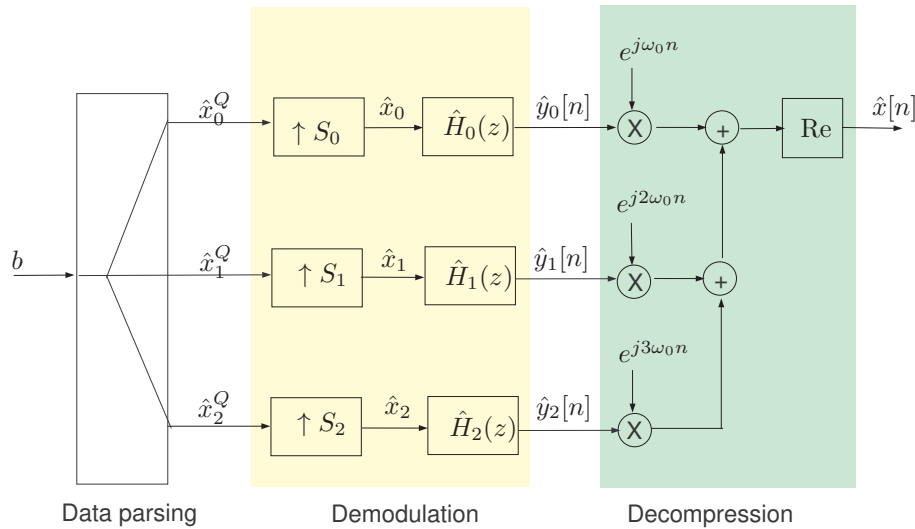


Fig. 4: A three-subband ASBC decoder. Time indices of internal signals are omitted with y_i standing for $y[n]$.

VII. EMPIRICAL STUDIES

We present in this section numerical results in two categories. The first category is the compression of high-density data from direct voltage measurements at the sampling rate of $F_s = 6$ KHz. Without compression, communicating this data stream to PDC or control center requires a 18kbps link for a single channel, assuming a 3 bit PCM quantization. The second category is the application of ASBC to direct PMU voltage and frequency measurements.

The standard performance measure for lossy compression is the *rate-distortion curve* that plots the signal reconstruction error (typically measured by mean-squared error) vs. the rate of compressed signal. To this end, we generalize the standard *total vector error (TVE)* on individual samples to one for finite-duration data streams. Referred to as *generalized TVE (G-TVE)*, the accuracy of the reconstructed data stream of length N is measured by

$$\text{G-TVE} = 10 \log_{10} \frac{\sum_{n=1}^N |x[n] - \hat{x}[n]|^2}{\sum_{n=1}^N x^2[n]} \quad (\text{dB}) \quad (4)$$

where $x[n]$ and $\hat{x}[n]$ represent the original and reconstructed signal respectively. Measured in decibels, G-TVE also has the interpretation to be the negative of signal-to-reconstruction noise ratio (SNR). Note that G-TVE reduces to TVE when $N = 1$.

The degree of compression is measured by compression ratio, which is defined as the ratio of uncompressed data rate $R^{\text{uncompressed}}$ and compressed data rate R^{SBC} . The data rates are calculated using

$$R^{\text{uncompressed}} = F_s R_0, \quad R^{\text{SBC}} = F_s \sum_{k=0}^K p_k \frac{R_k}{M_k} \quad (5)$$

where F_s represents the sampling frequency of the uncompressed data, R_k the quantization for the k th subband, p_k the probability of k th subband being active, and M_k the downsampling rate of k th subband. When the same quantization scheme is used for all subbands, the *compression ratio* is given by

$$\eta = \frac{R_0}{R_k} = \left(\sum_{k=0}^K p_k \frac{R_k}{R_0 M_k} \right)^{-1}. \quad (6)$$

In highlighting the tradeoff between compression rate and reconstruction error, the information theoretic measure for lossy compression is the rate-distortion plot that plot the rate of compression against reconstruction error [38]. For convenience, we used the inverse rate-distortion plot that shows the change of reconstruction error measured by NMSE or TVE with the inverse of compression ratio η^{-1} .

A. Compression of Direct Voltage Measurements.

We applied ASBC directly to a data set (henceforth referred to as UTK6K) provided the University of Tennessee, Knoxville. The UTK6K data set consisted of

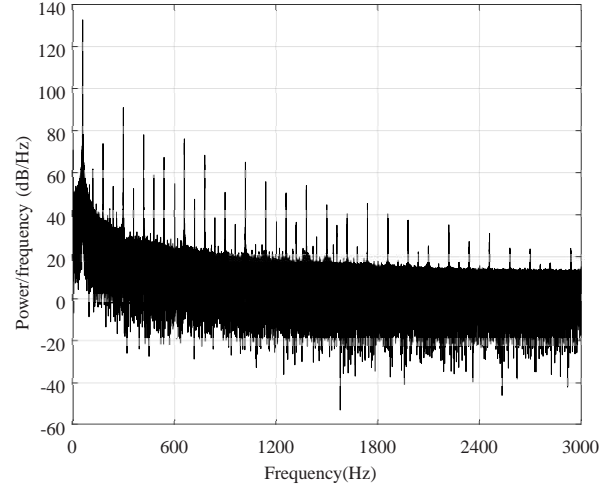


Fig. 5: Power spectrum density of the voltage measurements sampled at 6 kHz.

1.8 million voltage measurements sampled at 6KHz. Fig. 5 shows the power spectrum of the data set, from which we observed the presence of significant harmonics.

ASBC was implemented with 3 Hz bandwidth for all harmonics, and we encoded 5,10,15,20,40 and 50 subbands. Fig.6 shows the the inverse rate-distortion figure of ASBC, which shows that encoding up to 20 harmonic subbands produced sufficient accuracy of reconstruction. Note that the bandwidth of each subband used in the experiment was uniform, and a better compression ratio would have been achieved by adaptively choosing the bandwidth for each subband.

Fig. 7 (Top) shows one segment of the original and the reconstructed signals. The trajectory is plotted with the first

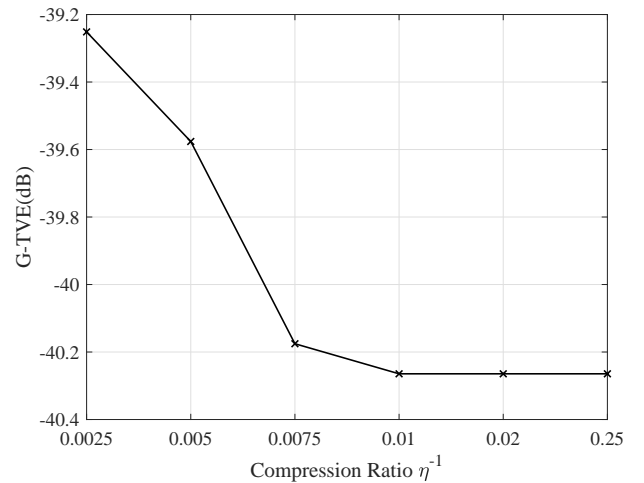


Fig. 6: Inverse rate-distortion curve with 3Hz bandwidth for all subbands.

20 subbands active, and each with 5Hz bandwidth, where ASBC was shown to be able to reconstruct the original signal with negligible reconstruction error from the compressed signal with high compression ratio. Fig. 7 (bottom) shows the normalized reconstruction error in the time domain.

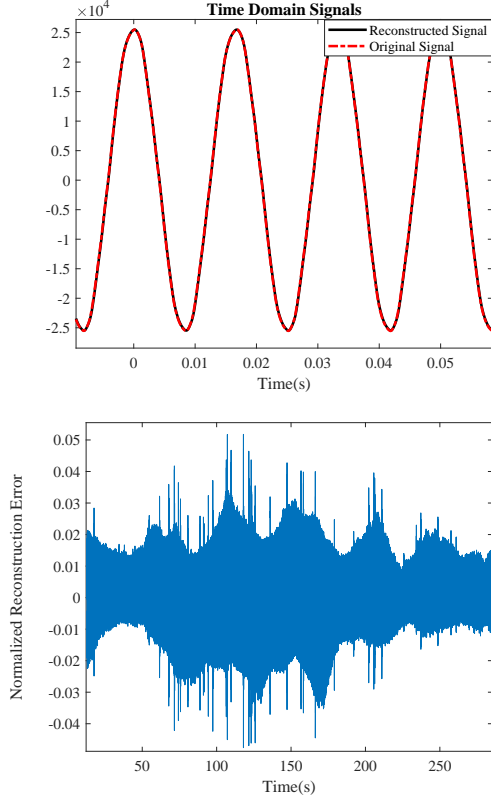


Fig. 7: Top: a segment of the original and reconstructed signal. Bottom: normalized reconstruction error.

Case Number	Maximum TVE(%)	G-TVE(dB)
1	0.95	-59.2382
2	0.76	-58.7235
3	0.82	-59.2657
4	0.71	-60.1384
5	0.81	-59.2062
6	0.72	-60.1303
7	0.74	-59.8744
8	1.08	-59.3843
9	0.77	-59.2343
10	0.79	-59.8777

TABLE I: TVE for the EPFL synchrophasor dataset. Compression ratio is 50:1. Subband filter with 1Hz bandwidth was used.

B. Compression of voltage phasor and frequency data

We applied ASBC to two datasets consisting of PMU phasor and frequency measurements. The first dataset, referred to as EPFL50, was the EPFL synchrophasor measurement of a local distribution system presented in [39]. The dataset consisted of 10 data streams, each containing 180,000 voltage phasor measurements at the 50 Hz frame rate. Some of the data streams had significant voltage fluctuations. The second dataset, referred to as UTK1.44, is a data set of frequency estimates from the University of Tennessee, Knoxville. The dataset contains two data streams, each with 1,800,000 samples. For both datasets, since there is no higher-order harmonics, only one subband ($k = 0$) of ASBC is used.

Table I shows the maximum TVE of the 10 data streams of the EPFL dataset at the 50:1 compression ratio. It can be observed that the maximum TVE for majority of the cases is under 1% which satisfies the requirement in [25].

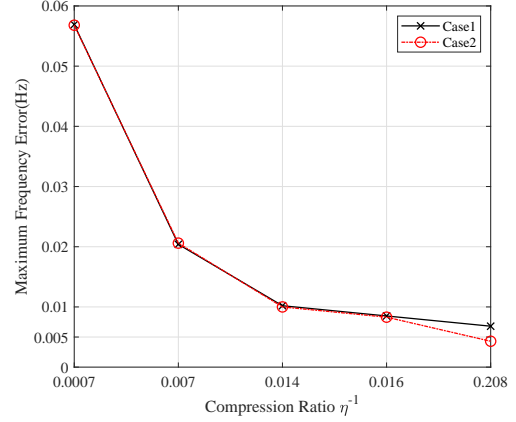


Fig. 8: The inverse rate-distortion curve for the compression of frequency measurement UTK1.44 dataset.

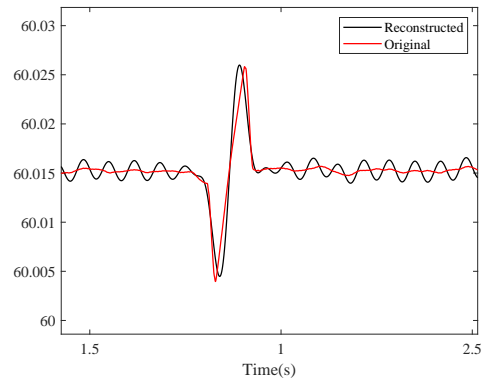


Fig. 9: The original and reconstructed frequency measurement during a frequency excursion.

Fig. 8 is the inverse ratet-distortion ratio that shows the maximum frequency error against compression ratio. The subband filter bandwidth was chosen to be 1Hz, 10Hz, 20Hz, and 24Hz. The maximum frequency reconstruction error was obtained during a frequency excursion. The 24 Hz bandwidth subband compression satisfied the IEEE standard C.71 dynamic compliance that requires that the maximum frequency error is below 0.01Hz for P class PMUs with reporting rate smaller than 20 Hz.

Fig. 9 presents the trajectory of the frequency measurement and its reconstruction during a frequency excursion event. The reconstructed signal is oscillating slightly before the deviation begins due to the windowing effect.

VIII. CONCLUSION

We have developed an adaptive subband compression (ASBC) technique for the streaming of measurement data of a wide-area measurement system. Different from existing technologies, ASBC employs a filter-bank that decomposes measurements based on the harmonic structure of the signal waveforms and adaptively compresses individual harmonic components. A prototype implementation of ASBC offers a significantly improved rate-distortion tradeoff.

REFERENCES

- [1] A. J. Calvaer and E. V. Geert, "Quasi steady state synchronous machine linearization around an operating point and applications," *IEEE Transactions on Power Apparatus and Systems*, vol. PAS-103, no. 6, pp. 1466–1472, June 1984.
- [2] U. Canada Power System Outage Task Force, "Final report on the august 14, 2003 blackout in the united states and canada: Causes and recommendations," 04 2004.
- [3] I. Dobson, B. A. Carreras, V. E. Lynch, and D. E. Newman, "Complex systems analysis of series of blackouts: Cascading failure, critical points, and self-organization," *Chaos: An Interdisciplinary Journal of Nonlinear Science*, vol. 17, no. 2, p. 026103, 2007. [Online]. Available: <https://doi.org/10.1063/1.2737822>
- [4] T. Van Cutsem, "Voltage instability: phenomena, countermeasures, and analysis methods," *Proceedings of the IEEE*, vol. 88, no. 2, pp. 208–227, Feb 2000.
- [5] V. Ajarapu and B. Lee, "Bibliography on voltage stability," *IEEE Transactions on Power Systems*, vol. 13, no. 1, pp. 115–125, Feb 1998.
- [6] J. S. Thorp, A. G. Phadke, and K. J. Karimi, "Real time voltage-phasor measurement for static state estimation," *IEEE Transactions on Power Apparatus and Systems*, vol. PAS-104, no. 11, pp. 3098–3106, Nov 1985.
- [7] A. G. Phadke, "Synchronized phasor measurements in power systems," *IEEE Computer Applications in Power*, vol. 6, no. 2, pp. 10–15, April 1993.
- [8] A. G. Phadke and J. Thorp, *Synchronized Phasor Measurements and Their Applications*. Springer, 2017.
- [9] J. De La Ree, V. Centeno, J. S. Thorp, and A. G. Phadke, "Synchronized phasor measurement applications in power systems," *IEEE Transactions on Smart Grid*, vol. 1, no. 1, pp. 20–27, June 2010.
- [10] D. Elizondo, R. M. Gardner, and R. Leon, "Synchrophasor technology: The boom of investments and information flow from north america to latin america," in *2012 IEEE Power and Energy Society General Meeting*, July 2012, pp. 1–6.
- [11] A. Chakraborty and P. P. Khargonekar, "Introduction to wide-area control of power systems," in *2013 American Control Conference*, June 2013, pp. 6758–6770.
- [12] S. M. Dibaji, A. Annaswamy, A. Chakraborty, and A. Hussain, "Sparse and distributed control of wide-area power systems with large communication delays," in *2018 Annual American Control Conference (ACC)*, June 2018, pp. 3822–3827.
- [13] F. Aminifar, M. Fotuhi-Firuzabad, A. Safdarian, A. Davoudi, and M. Shahidehpour, "Synchrophasor measurement technology in power systems: Panorama and state-of-the-art," *IEEE Access*, vol. 2, pp. 1607–1628, 2014.
- [14] J. L. Rueda-Torres and F. Gonzalez-Longatt, *Introduction: The Role of Wide Area Monitoring Systems in Dynamic Vulnerability Assessment*. IEEE, 2018, pp. 1–19. [Online]. Available: <https://ieeexplore.ieee.org/document/8292917>
- [15] C. Liu, J. S. Thorp, J. Lu, R. J. Thomas, and H. Chiang, "Detection of transiently chaotic swings in power systems using real-time phasor measurements," *IEEE Transactions on Power Systems*, vol. 9, no. 3, pp. 1285–1292, Aug 1994.
- [16] J. F. Hauer, D. J. Trudnowski, and J. G. DeSteese, "A perspective on wams analysis tools for tracking of oscillatory dynamics," in *2007 IEEE Power Engineering Society General Meeting*, June 2007, pp. 1–10.
- [17] D. Novosel, V. Madani, B. Bhargava, K. Vu, and J. Cole, "Dawn of the grid synchronization," *IEEE Power and Energy Magazine*, vol. 6, no. 1, pp. 49–60, January 2008.
- [18] M. Parashar and J. Mo, "Real time dynamics monitoring system (rtdms): Phasor applications for the control room," in *2009 42nd Hawaii International Conference on System Sciences*, Jan 2009, pp. 1–11.
- [19] M. Glavic and T. Van Cutsem, "Wide-area detection of voltage instability from synchronized phasor measurements. part i: Principle," *IEEE Transactions on Power Systems*, vol. 24, no. 3, pp. 1408–1416, Aug 2009.
- [20] —, "Wide-area detection of voltage instability from synchronized phasor measurements. part ii: Simulation results," *IEEE Transactions on Power Systems*, vol. 24, no. 3, pp. 1417–1425, Aug 2009.
- [21] —, "A short survey of methods for voltage instability detection," in *2011 IEEE Power and Energy Society General Meeting*, July 2011, pp. 1–8.
- [22] M. H. J. Bollen, S. Cundeva, S. K. Rnnberg, M. Wahlberg, K. Yang, and L. Yao, "A wind park emitting characteristic and non-characteristic harmonics," in *Proceedings of 14th International Power Electronics and Motion Control Conference EPE-PEMC 2010*, 2010, pp. S14–22–S14–26.
- [23] R. Teodorescu, M. Liserre, and P. Rodriguez, *Grid converters for photovoltaic and wind power systems*. John Wiley & Sons, Ltd.
- [24] IEEE, "IEEE standard for interconnection and interoperability of distributed energy resources with associated electric power systems interfaces," *IEEE Std 1547-2018 (Revision of IEEE Std 1547-2003)*, pp. 1–138, April 2018.
- [25] —, "IEEE standard for synchrophasor data transfer for power systems," *IEEE Std C37.118.2-2011 (Revision of IEEE Std C37.118-2005)*, pp. 1–53, Dec 2011.
- [26] K. Mehta and B. D. Russell, "Data compression for digital data from power systems disturbances: requirements and technique evaluation," *IEEE Transactions on Power Delivery*, vol. 4, no. 3, pp. 1683–1688, July 1989.
- [27] T. B. Littler and D. J. Morrow, "Wavelets for the analysis and compression of power system disturbances," *IEEE Transactions on Power Delivery*, vol. 14, no. 2, pp. 358–364, April 1999.
- [28] S. Santoso, E. J. Powers, and W. M. Grady, "Power quality disturbance data compression using wavelet transform methods," *IEEE Transactions on Power Delivery*, vol. 12, no. 3, pp. 1250–1257, July 1997.
- [29] A. M. Gaouda, M. M. A. Salama, M. R. Sultan, and A. Y. Chikhani, "Application of multiresolution signal decomposition for monitoring short-duration variations in distribution systems," *IEEE Transactions on Power Delivery*, vol. 15, no. 2, pp. 478–485, April 2000.
- [30] S. Santoso, E. J. Powers, W. M. Grady, and A. C. Parsons, "Power quality disturbance waveform recognition using wavelet-based neural classifier. i. theoretical foundation," *IEEE Transactions on Power Delivery*, vol. 15, no. 1, pp. 222–228, Jan 2000.
- [31] P. K. Dash, B. K. Panigrahi, D. K. Sahoo, and G. Panda, "Power quality disturbance data compression, detection, and classification using integrated spline wavelet and s-transform," *IEEE Transactions on Power Delivery*, vol. 18, no. 2, pp. 595–600, April 2003.
- [32] N. C. F. Tse, J. Y. C. Chan, W. Lau, J. T. Y. Poon, and L. L. Lai, "Real-time power-quality monitoring with hybrid sinusoidal and lifting wavelet compression algorithm," *IEEE Transactions on Power Delivery*, vol. 27, no. 4, pp. 1718–1726, Oct 2012.

- [33] S. Meher, A. Pradhan, and G. Panda, "An integrated data compression scheme for power quality events using spline wavelet and neural network," *Electric Power Systems Research*, vol. 69, pp. 213–220, 05 2004.
- [34] W. R. A. Ibrahim and M. M. Morcos, "Novel data compression technique for power waveforms using adaptive fuzzy logic," *IEEE Transactions on Power Delivery*, vol. 20, no. 3, pp. 2136–2143, July 2005.
- [35] Y. Ge, A. J. Flueck, D. Kim, J. Ahn, J. Lee, and D. Kwon, "Power system real-time event detection and associated data archival reduction based on synchrophasors," *IEEE Transactions on Smart Grid*, vol. 6, no. 4, pp. 2088–2097, July 2015.
- [36] M. P. Tcheou, L. Lovisolo, M. V. Ribeiro, E. A. B. da Silva, M. A. M. Rodrigues, J. M. T. Romano, and P. S. R. Diniz, "The compression of electric signal waveforms for smart grids: State of the art and future trends," *IEEE Transactions on Smart Grid*, vol. 5, no. 1, pp. 291–302, Jan 2014.
- [37] A. Gersho and R. M. Gray, *Vector Quantization and Signal Compression*. USA: Kluwer Academic Publishers, 1991.
- [38] T. Cover and J. Thomas, *Elements of Information Theory*. John Wiley & Sons, Inc., 1991.
- [39] M. Pignati, M. Popovic, S. Barreto, R. Cherkaoui, G. Dario Flores, J. Le Boudec, M. Mohiuddin, M. Paolone, P. Romano, S. Sarri, T. Tesfay, D. Tomozei, and L. Zanni, "Real-time state estimation of the epfl-campus medium-voltage grid by using pmus," in *2015 IEEE Power Energy Society Innovative Smart Grid Technologies Conference (ISGT)*, Feb 2015, pp. 1–5.